Kateryna_Kon - Stock.adobe.com

Therapeutic Potential of Green, Synthesized Gold Nanoparticles

SATABDI RAUTRAY AND A. USHA RAJANANTHINI

ABSTRACT

Gold nanoparticles (AuNPs) are important components for biomedical applications and are widely employed for diagnostics and therapeutics. Nanoparticles are mainly synthesized through chemical and physical methods, which are often costly and potentially harmful. Synthesis of nanoparticles using plants, however, is less toxic and more effective. Recently, researchers have been focusing on green synthesis of AuNPs. This study aims to use plant-leaf extract for the green synthesis of AuNPs and to evaluate their antibacterial and antioxidant activity. The results indicated that AuNPs can be synthesized using a simple method with extracts from *Adiantum capillus veneris* (ACV) and *Pteris quadriureta* (PQ) leaves. The characterization of the AuNPs was done by ultraviolet-visible spectroscopy, powder X-ray diffraction, Fourier transform infrared spectroscopy, and energy dispersive X-ray spectroscopy. The nanoparticles of ACV and PQ were seen at the wave length of 573 nm and 520 nm, respectively. The nanoparticles of both ACV and PQ leaves extract showed antioxidant, antibacterial, and antifungal activities. ACV nanoparticles showed increased antioxidant and antimicrobial activity compared to PQ. Taken together, the results reveal that the AuNPs synthesized from leaves of ACV and PQ possesses antioxidant and antimicrobial activity.

Nanotechnology is the most active area of research in the field of biotechnology (1). Nanobiotechnology applies the nanoscale principle to help understand and modify biosystems, including living and non-living, by using biological materials to make new strategies (2). Several methods are applied to synthesize nanoparticles including chemical, physical, electrochemical, sonochemical, irradiation, and biological methods. Among these, biological methods, by way of microorganisms (microbial nanosynthesis) and plants (phytonanosynthesis), are the most preferable. The synthesis of nanoparticles using plant extract provides advancement over other methods because it is simple, one step, cost-effective, environmentally friendly, relatively easy to reproduce, less toxic, and more effective (3–6).

Nanoparticles show novel and improved properties based on particular characteristics, such as size, distribution, and morphology (7). Metal nanoparticles, especially gold nanoparticles (AuNPs), show tremendous therapeutic potential against pathogens (8–10). The sizes of AuNPs vary from 1 nm to 8 µm, and the shapes are spherical, octahedral, sub-octahedral, decahedral multiple twinned, icosahedral multiple twinned, irregular shape, nanotriangles and nanoprisms, tetrahedral, hexagonal platelets, and nanorods (11–12). Researchers in the fields of medicine, cosmetology, biology, clinical chemistry, and pharmacology (13–17) have focused their attention on AuNP synthesis because of the particles' distinctive properties, including physiochemical and biological (18–20). Gold nanoparticles are also used for the diagnosis and treatment of several diseases, such as diabetes, cancer, Parkinson's, Alzheimer's, HIV/AIDS, tuber-

A. Usha Rajananthini, biotechurn@gmail.com, and **Satabdi Rautray**, rautray.satabdi@gmail.com, are with the Department of Biotechnology, Mother Teresa Women's University, Kodaikanal, Tamil Nadu, India.

Correspondence should be addressed to both authors.

PEER-REVIEWED

Submitted: July 30, 2019.
Accepted: Oct. 15, 2019.

Figure 1. Biosynthesis of gold nanoparticles (GNPs): A) auric chloride (HAuCl4) solution, B) extract, C) synthesized GNP in ruby red color solution.

culosis, and cardiovascular diseases, based on their biocompatibility and non-cytotoxicity (21–25).

In a previous study, the researchers of this study provided compelling evidence for the antioxidant and antimicrobial activities of the crude extracts of *Adiantum capillus veneris* (ACV) and *Pteris quadriureta* (PQ) (26). In the present study, researchers synthesized the AuNPs from the extract of ACV and PQ leaves by a green biological route and characterized them using ultraviolet-visible (UV-Vis) spectroscopy, energy dispersive X-ray spectroscopy (EDX), X-ray diffraction (XRD), and Fourier transform infrared spectroscopy (FTIR) analysis. Furthermore, the antioxidant and antimicrobial properties of the synthesized nanoparticles were examined.

MATERIALS AND METHODS

Collection, identification, and processing of plants

The leaves of ACV and PQ plants were collected from Kodaikanal hills, Tamil Nadu, India. The plants were identified by Regional Plant Resource Centre, Odisha Biodiversity Board (No. 2175). The plant leaves were washed thoroughly thrice with distilled water, shade dried for five days, and blended into a fine powder. The leaf powder was sterilized at 121 °C for 15 min. Next, 20 g of powder was mixed with 200 mL of distilled water and kept in a boiling water bath at 60 °C for 10 min. The extracts were filtered (Whatman filter paper No. 1), and the filtered extract was stored in the refrigerator at 4 °C for further studies.

Synthesis of AuNPs and visual analysis

For the biosynthesis of AuNPs, 1.5 mL of plant extract powder was mixed with 30 mL of auric chloride solution (1 mM/mL) and incubated at 28 °C for 24 h. The color change in reaction mixture (auric chloride solution + leaf extract) was recorded through visual observation. The bioreduced gold nanoparticle solution was filtered (Whatmann No.1 filter paper), and the bioreduction of pure gold ions was observed at different time intervals by monitoring the UV-Vis spectrum of the solution between 500 nm to 600 nm using a spectrophotometer (Thermo-Biomate 3 UV-visible spectrophotometer).

X-ray diffraction measurements

The completely bioreduced sample was concentrated in an oven at 50 °C, and the concentrated solution was then centrifuged at 6000 rpm for 15 min. The obtained pellet was washed and redispersed in deionized water. The dried mixture of AuNPs was collected to determine the formation of AuNPs by XRD operated at a voltage of 30 kV and a current of 30 mA with Copper K-alpha radiation in a θ–2θ configuration.

Determination of crystalline size

Average crystallite size of gold was calculated using Scherrer's formula (**Equation 1**):

$$D = k\lambda / \beta\cos\theta \qquad \text{[Eq. 1]}$$

Where D = average crystallite size, k = constant, λ = X-ray wavelength, β = angular full width at half maximum (FWHM) of the XRD peak at the diffraction angle, and θ = diffraction angle.

FTIR analysis

FTIR spectra of the aqueous leaf extract and AuNP samples were analyzed by FTIR spectroscopy (Hitachi). The FTIR analysis was performed with potassium bromide (KBr) pellets and recorded in the range of 400 cm^{-1}–4000 cm^{-1}. The various modes of vibrations were identified and assigned to determine the different functional groups present in the samples.

Figure 2. Ultraviolet spectrum of *Adiantum capillus veneris* (ACV) and *Pteris quadriureta* (PQ) synthesized gold nanoparticles (GNPs).

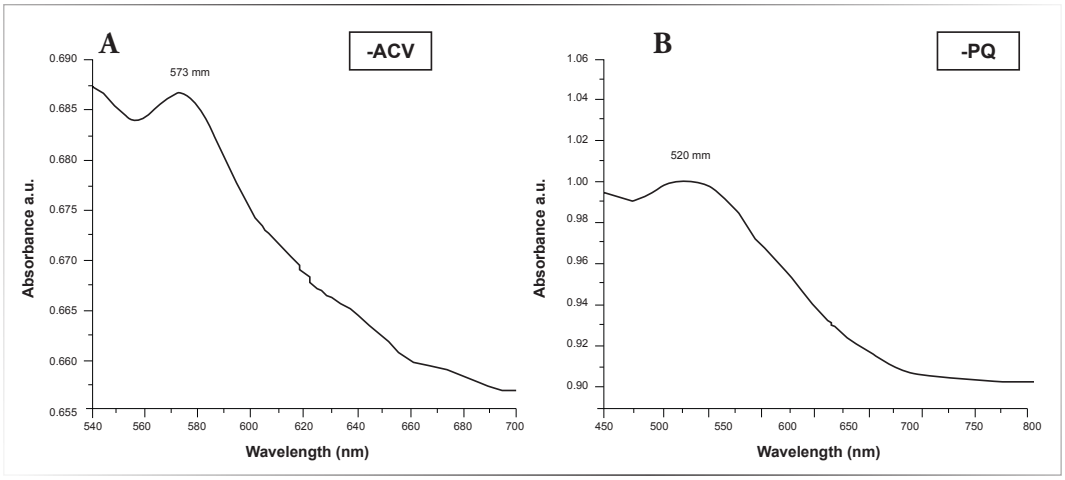

EDX analysis

Scanning electron microscope (SEM) (JSM-5800 LV, JEOL) was used to determine the shape of developed nanoparticles. Samples were prepared by depositing a drop of colloidal solution on an aluminium grid sample holder and drying at room temperature. Elemental composition of the sample was analyzed with energy dispersive analysis of EDX coupled to the SEM.

DPPH radical scavenging assay

Free radical scavenging activity of the nanoparticles was analyzed by a 2,2-diphenyl-1-picryl-hydrazyl-hydrate (DPPH) assay. Different concentrations (10–80 µg/mL) of AuNPs were added in equal volume to 0.1 mM methanolic DPPH solution. After 30 minutes of incubation at room temperature, absorbance of the samples was read at 517 nm. Ascorbic acid was used as a standard. The experiment was repeated in triplicate, and the DPPH scavenging activity was calculated by percent inhibition (**Equation 2**):

$$\text{Inhibition percent} = [(A_0 - A_1)/ A_0] \times 100 \quad \text{[Eq. 2]}$$

where A_0 is the absorbance of the control and A_1 the absorbance of the NPs solution.

Hydroxyl radical assay

The hydroxyl radical scavenging activity of AuNPs of ACV and PQ was evaluated by hydroxyl radical assay (27). The reaction mixture containing dilution series from 10 µg/mL to 100 µg/mL of AuNPs was incubated with deoxyribose (3.75 mM), hydrogen peroxide (H_2O_2) (1 mM), iron (III) chloride (FeCl3) (100 µM) in phosphate buffer (pH 7.4). The reaction was terminated by thiobarbituric acid (1 mL; 1% w/v) and trichloroacetic acid (1 mL; 2% w/v) and then heated in a boiling water bath for 15 min. Pink chromagen was formed, which eventually resulted in the formation of thiobarbituric acid reactive substances (TBARS). The content was cooled, and absorbance of mixture was measured at 535 nm against a blank. The percent inhibition of hydroxyl radical generation was calculated using **Equation 3**:

$$\text{Inhibition percent} = [(C–T/C)] \times 100 \quad \text{[Eq. 3]}$$

where *C* is absorbance of the control and *T* is the test samples.

Superoxide radical-scavenging assay

The superoxide radical scavenging activity of AuNPs from ACV and PQ was evaluated by superoxide radical scavenging assay. The reaction mixture was made up of 3 mL (50 mM sodium phosphate buffer [pH 7.6], 20 µg riboflavin, 12 mM ethylenediaminetetraacetic acid [EDTA]), 0.1 mg nitro blue tetrazolium (NBT), and 100 µl sample solution. The reaction mixture was incubated for 90 s, and, immediately after illumination, the absorbance was measured at 590 nm. The entire reaction assembly was enclosed in a box lined with aluminium foil. Identical tubes with reaction mixture kept in the dark served as blanks. The percentage inhibition of superoxide

Figure 3. X-ray diffraction (XRD) analysis of A) *Adiantum capillus veneris* (ACV) and B) *Pteris quadriureta* (PQ)-synthesized gold nanoparticles (GNPs). Crystalline nanoparticles represented by four peaks corresponding to standard Bragg reflections (111), (200), (220), and (311) of face centers cubic lattice.

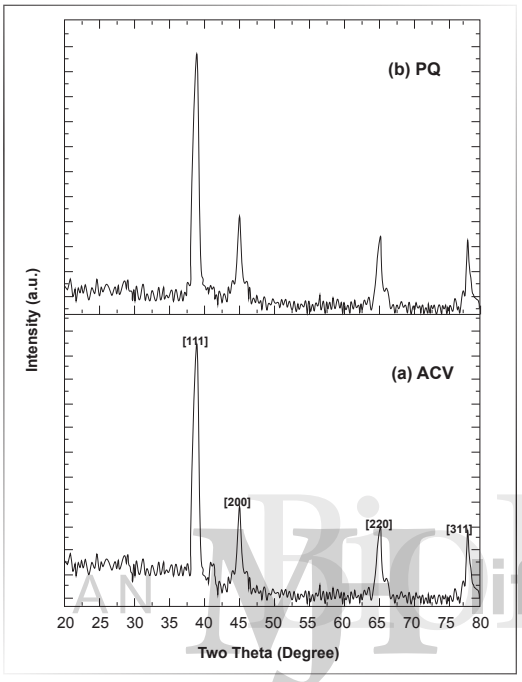

anion generation was calculated as shown in **Equation 4**:

$$\% \text{ inhibition} = [(A_0 - A_1)/A_0] \times 100 \quad \text{[Eq. 4]}$$

where A_0 is the absorbance of the control, and A_1 is the absorbance of the sample extract and standard (28).

Measurement of hydrogen peroxide scavenging activity

The ability of AuNPs to scavenge H_2O_2 was determined according to the method of Ruch *et al.* (29) with slight modifications. The mixture was made up of different concentrations of AuNPs (10–80 µg/mL), and butylated hydroxytoluene(BHT) was mixed with 2.4 mL of phosphate buffer (0.1 M, pH 7.4) and 0.6 mL of H_2O_2 solution (40 mM). Then the mixture was vortexed and incubated at room temperature for 10 min. At the end of incubation, the concentration of H_2O_2 was determined by absorbance at 230 nm against a blank solution containing phosphate buffer without H_2O_2. The H_2O_2 scavenging ability was calculated using the formula as described for DPPH assay (**Equation 2**).

Antimicrobial activity

Bacteria such as *Escherichia coli*, *Pseudomonas aeruginosa*, *Salmonella enteric*, *Staphylococcus aureus*, and *Bacillus subtilis* and fungi such as *Trichophytonrubrum*, *Scedosporiumapiospermum*, *Aspergillus fumigates*, *Aspergillusniger*, and *Aspergillusflavus* were collected and clinically isolated. Each bacterial strain was suspended in a nutrient broth and incubated for 18 h at 37 °C. Nutrient agar (NA) and potato dextrose agar (PDA) were used for the study of antibacterial activity and antifungal activity, respectively. The nutrient-broth-cultured bacteria were spread over a NA plate, whereas a 24-h cultured fungi was spread on PDA by using cotton swab. A 5-mm disc was dipped in each nanoparticle solution, including a positive control solution, such as ampicillin and itraconazole (10 µg), for bacteria and fungi, respectively, and placed on the swabbed agar plate. Each disc absorbed 15 µl of sample, which is made up of 50 mg/mL and 100 mg/mL concentrations. The plates were then incubated at 37 °C for 24 h for bacterial pathogens and 72 h for fungal pathogens. The antimicrobial activity was evaluated by measuring the diameter of the inhibition zone.

Statistical analysis

The data of various analyses were expressed as mean ± standard deviation. All tests were carried out in triplicate to improve the accuracy.

RESULTS

UV analysis

The formation of purple color (**Figure 1C**) after mixing the plant extracts with auric chloride (HAuCl4) solution showed the presence of AuNPs. **Figure 1A** shows the HAuCl4 solution, **Figure 1B** is the aqueous extract solution of the plant, and **Figure 1C** is the gold nanoparticle-synthesized solution. **Figure 2** shows the UV-Vis absorption spectra of synthesized AuNPs. The UV-Vis analysis (**Figure 2**) also confirmed the formation of AuNPs at a wavelength of 573 nm and 520 nm of ACV and PQ plant extracts, respectively.

XRD analysis

The X-ray diffraction pattern (XRD) revealed that AuNPs of ACV and PQ are crystalline in nature. The Debye–Scherrer's equation was used

Figure 4. Fourier transform infrared spectroscopy (FTIR) analysis showing absorption spectra of gold nanoparticles synthesized from leaves of A) *Adiantum capillus veneris* (ACV) and B) *Pteris quadriureta* (PQ).

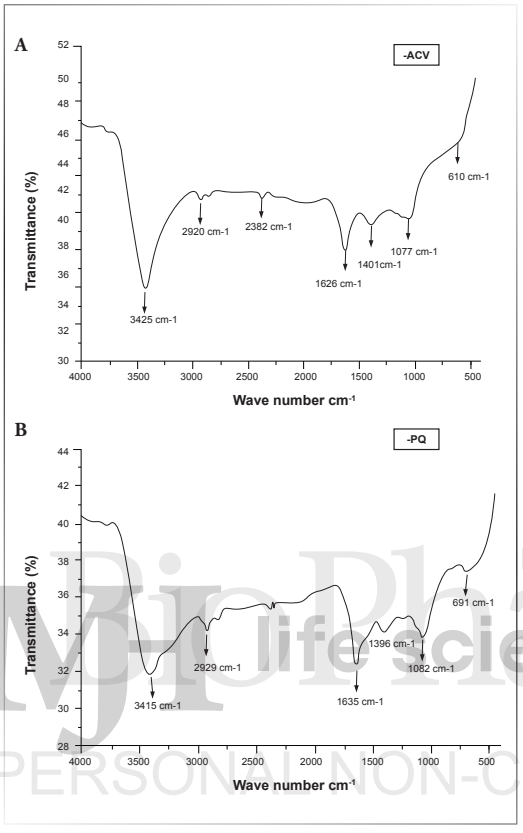

to calculate the size of the AuNPs on the basis of the FWHM of the (111) Bragg's reflection arising from the diffractograms. The intensity of the peaks of ACV of (111) at 38.91° diffraction was much stronger than those peaks of (200), (220), and (311) at 45.02°, 65.34°, and 78.24°, respectively, and the intensity of the peaks of PQ of (111) at 38.92° diffraction was much stronger than those peaks of (200), (220), and (311) at 45.08°, 65.36°, and 78.26°, respectively. The Bragg reflections of lattice planes showed the face-centered cubic structures for gold, and the broadening of Bragg's peaks indicates the formation of nanoparticles. A few additional and unassigned peaks were also observed, which resulted because of bio-organic compounds or proteins in the nanoparticle during the synthesis. These unassigned peaks did not interfere with the Bragg reflection peaks but showed the synthesis of AuNPs, and they played a role in the stabilization of AuNPs (**Figure 3**).

FTIR analysis

FTIR analysis was done to detect the possible biomolecules which play a role in the reduction of AuNPs following the stabilization-capping. **Figure 4** shows the FTIR spectra of the ACV and PQ leaf extract and AuNPs. We found strong bands at 3425 cm^{-1}, 2920 cm^{-1}, 2382 cm^{-1}, 1626 cm^{-1}, and 1401 cm^{-1} of ACV extract along with a few weak bands, including 1077 cm^{-1} and 610 cm^{-1}. In the case of PQ, it showed strong bands at 3416 cm^{-1}, 2929 cm^{-1}, 1635 cm^{-1}, 1396 cm^{-1} and weak bands at 1082 cm^{-1} and 691 cm^{-1}. Bands at 3425 cm^{-1} and 3416 cm^{-1} correspond to O–H stretching modes from alcohol and phenol groups, while bands at 2920 cm^{-1} and 2929 cm^{-1} belong to saturated systems alkanes. Bands at 2382 cm^{-1} arise because of the stretching of C–C of the alkyne group, and bands at 1626 cm^{-1} and 1635 cm^{-1} arise because of the C=O functional group of amide in stretching mode. Bands at 1401 cm^{-1} and 1396 cm^{-1} belong to the methylene group, whereas the weakest bands, including 1077 cm^{-1} and 1082 cm^{-1} as well as 610 cm^{-1} and 691 cm^{-1} correspond to the C–O–C functional group and arenes group, respectively.

Energy dispersive X-ray analysis

EDX analysis confirmed the presence of AuNPs of ACV and PQ plant extracts, which accounted for 41.85% and 48.23% by weight of ACV- and PQ-analyzed samples, respectively. A strong and clear peak of gold atoms was observed in the spot-directed EDX spectrum of all the AuNPs of both the plant extracts. In the case of ACV, oxygen (O), manganese, potassium (K), chloride (Cl), and calcium atoms were indicated by the weaker signals. In the case of PQ, O, K, silicon, and Cl atoms were also shown by the weaker peaks, which may have resulted from X-ray emissions from proteins/enzymes present in the biomolecules, which can cause capping of the AuNPs (**Figure 5**).

Antioxidant activity

The ACV and PQ nanoparticles exhibited free radical scavenging activities, with the ACV nanoparticles exhibiting the highest activity, followed by PQ nanoparticle activity. At concentrations of 10 µg/mL to 200 µg/mL, the scavenging activities of ACV were 35% to 91%, while the scavenging activities of PQ were 22% to 81% (**Figure 6A**). Further, the superoxide radical scavenging activity of the ACV nanoparticles was found to be significantly higher than that of the PQ nanoparticles (**Figure 6B**).

Figure 5. Energy dispersive X-ray spectroscopy (EDX) analysis of gold nanoparticles (AuNPs) produced using aqueous plant extracts, A) *Adiantum capillus veneris* (ACV) and B) *Pteris quadriureta* (PQ). In all cases, peaks are labeled. Gold is detected in all, consistent with the formation of AuNPs, while the other elements come from trace elements in the extracts.

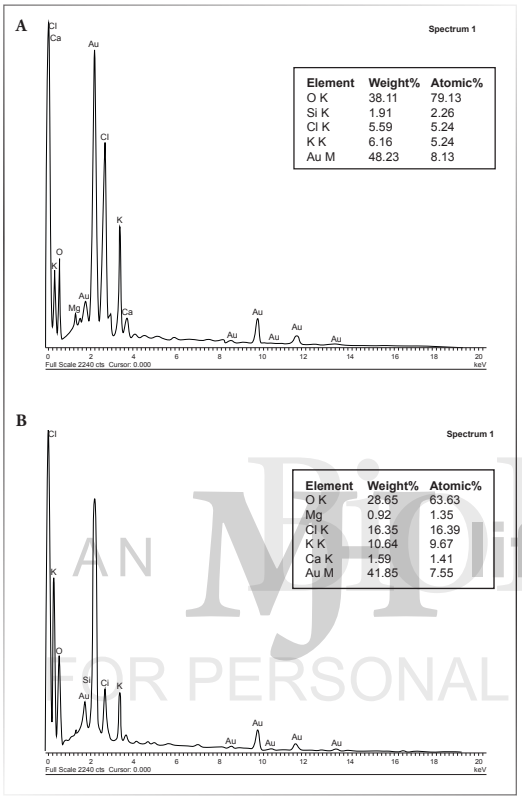

Antioxidant potential of the ACV and PQ nanoparticles was further estimated using hydroxyl radical scavenging activity. It was observed that the scavenging activity of nanoparticles of ACV and PQ was increased from 31% to 85% and 20% to 74%, respectively, at concentrations of 10 µg/mL to 200 µg/mL (**Figure 6C**). The scavenging ability of nanoparticles of ACV and PQ on H_2O_2 is shown **Figure 6D**. The nanoparticles of ACV and PQ were capable of scavenging H_2O_2 in a dose-dependent manner.

Antimicrobial activity

Tables I and **II** show the antibacterial and antifungal activities of nanoparticles of ACV and PQ leaves. Two concentrations (50 mg/mL and 100 mg/mL) of nanoparticles were tested against five different bacteria (*B. subtilis*, *E. coli*, *P. aeruginosa*, *S. enteric*, and *S. aureus*) and five different fungi (*A. niger*, *A. fumigates*, *A. flavus*, *T. rubrum*, and *S. apiospermum*). There was a significant increase in the zone of inhibition as the concentration of AuNPs increased (**Figures 7A and 7B**).

DISCUSSION

Medicinal plants are in demand because of their biological properties and bioactive compounds, which are known to act against various diseases (30–32);. The green synthesized nanoparticles have attracted global attention because of their unique properties and because they have fewer side effects (33). The present study suggests that nanoparticles of ACV and PQ leaves possess antioxidant, antibacterial, and antifungal activities that can be therapeutically beneficial.

The presence of gold nanoparticles was confirmed by change of color from the reduction of Au+ to Au0 ions at altered time intervals. The UV-Vis spectra showed strong peaks for ACV extracts at 573 nm and for PQ extracts at 520 nm. The formation of these strong, broad peaks has been found for various AuNPs with sizes ranging from 2 nm to 100 nm (34). Jayaseelan *et al.*, (2013) has reported that aqueous extract of *Abelmoschus esculentus* seeds showed surface plasmon resonance at 536 nm (35).

In XRD analysis, strong peaks of both the nanoparticles were observed at range of 2θ values of

Table I. Anti-bacterial activity of *Adiantum capillus veneris* (ACV) and *Pteris quadriureta* (PQ) gold nanoparticles. Values are means of triplicate determinations (n=3) ± standard deviation.
***** ($p<0.05$) significantly different from antibiotic.

Bacteria	Antibiotic (zone of inhibtion in mm)	ACV	PQ
Bacillus subtilis	24.00	17.00	16.00
Escherichia coli	26.00	21.00	17.00
Pseudomonas aeruginosa	22.00	18.00	16.00
Salmonella enteric	21.00	16.00	16.00
Staphylococcus aureus	39.00	19.00	18.00

Figure 6. Anti-oxidant activity of *Adiantum capillus veneris* (ACV) and *Pteris quadriureta* (PQ) gold nanoparticles (AuNPs). A shows 2,2-diphenyl-1-picryl-hydrazyl-hydrate (DPPH) free radical scavenging activity; B shows superoxide radical scavenging activity; C shows hydroxyl radical scavenging activity; and D shows hydrogen peroxide (H2O2) scavenging activity. Values are means of triplicate determinations (n = 3) ± standard deviation. Ascorbic acid was used as standard.

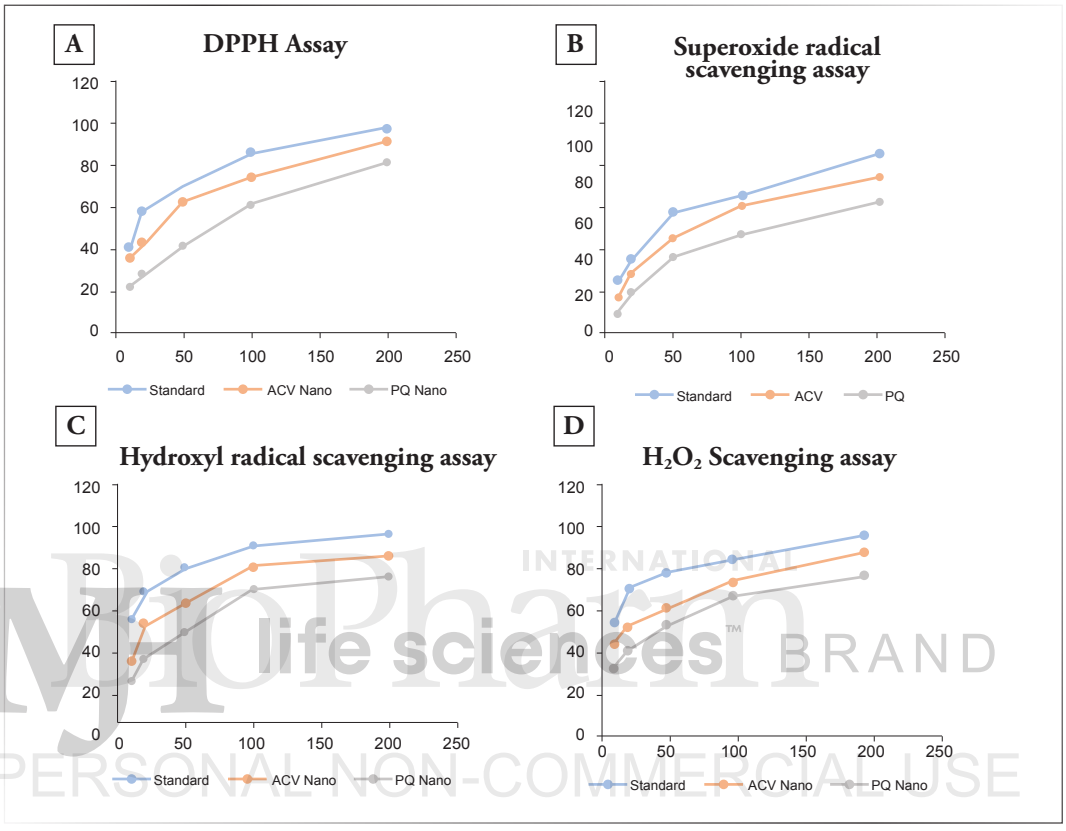

38.91, which corresponded to the Bragg's reflections of (111), (200), (220), and (311). FTIR analysis of the ACV and PQ leaves' extracts indicated that the carboxyl groups (C=O), hydroxyl groups (OH), and amine groups (N-H) of both plant extracts are mainly involved in the reduction of Au+ nanoparticles to Au0 nanoparticles by acting on the C–C bond in the alkyne group. Similar results were described by other studies, in which it was reported that the vibrational bending of the peaks may have occurred from the presence of compounds in the plant extracts, including flavonoids, terpenoids, alkaloids, and soluble proteins. The presence of these compounds in the extracts may also cause the stabilization of gold nanoparticles (36). The EDX profile of AuNPs of ACV and PQ showed strong signals for gold atoms and weak signals for O, K, Si, and Cl atoms. The presence of these characteristic

Table II. Anti-fungal activity of *adiantum capillus veneris* (ACV) and *Pteris quadriureta* (PQ) gold nanoparticles. Values are means of triplicate determinations (n=3) ± standard deviation.
***** ($p<0.05$) significantly different from antibiotic.

Fungi	Antibiotic (zone of inhibtion in mm)	ACV	PQ
Aspergillus niger	24.00	20.00	16.00
Aspergillus fumigates	25.00	16.00	15.00
Aspergillus flavus	24.00	20.00	15.00
Trichophyton rubrum	29.00	17.00	14.00
Scedosporium apiospermum	30.00	16.00	15.00

Figure 7. A. Anti-bacterial and **B.** anti-fungal activity of aqueous extracts of *Adiantum capillus veneris* (ACV) and *Pteris quadriureta* (PQ) leaves; a. control, b. positive control, c. gold nanoparticles.

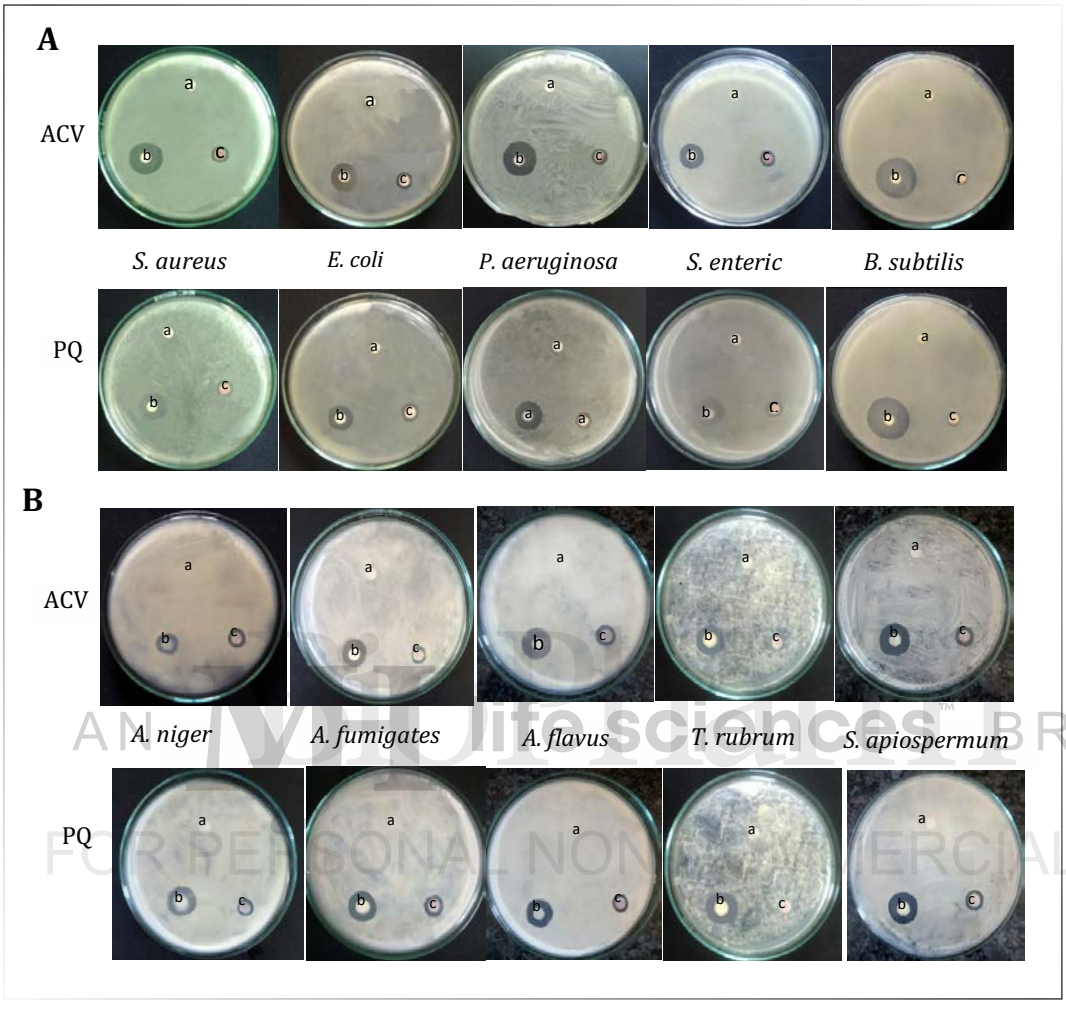

peaks of gold nanoparticles shows the effective combination of polyphenolics on the outer surface of the gold nanoparticles (37–39).

DPPH and superoxide radical scavenging activity are widely used for testing preliminary radical scavenging activity of compounds or nanoparticles and provide easy and rapid evaluation. In the present study, the synthesized AuNPs exhibited potential free radical scavenging activity against both DPPH and superoxide radicals. The presence of polyphenolic compounds such as flavonoids, flavonols, proanthocyanidin, and phenolics in plants have been reported to have strong antioxidant activities, which help to protect cells against oxidative damage by free radicals (40). It was reported that the antioxidant activities of plant extracts were enhanced by conversion into gold nanoparticles (41).

The hydroxyl radical formed in the Fenton reaction in the presence of reduced transition metals is known to be the most reactive of all the reduced forms of dioxygen and is capable of damaging of almost every molecule found in living cells (42). An increase in hydroxyl radical scavenging activities with increasing concentrations of nanoparticles was observed in this study. Medhe *et al.* (2014) reported that dihydroxy flavone-coated nanoparticle showed increased hydroxyl radical scavenging activity (43). In addition, the gold nanoparticles of ACV and PQ exhibited increased H_2O_2 scavenging activity. H_2O_2 scavenging by phytochemicals may be attributed to the donation of electrons to H_2O_2, thus neutralizing it to water (44).

AuNPs synthesized by natural compounds extracted from plants are gaining importance. The nanoparticles of ACV and PQ were very effective in inhibiting microbial growth, which may be due

to the presence of sterols and secondary metabolites. AuNPs were found to be toxic for microbial organisms (45–48). Sreelakshmi *et al.* (2011) reported that AuNPs synthesized by using natural honey showed increased antimicrobial activity (49). Zhang *et al.* (2016) reported that green-synthesized AuNPs show efficient antibacterial activity compared to chemically synthesized AuNPs, which showed nearly no antimicrobial activity (50–51).

The present study demonstrates an eco-friendly and low-cost method for biosynthesis of AuNPs from ACV and PQ. This method of reduction used here is simple, easy to perform, inexpensive, and eco-friendly as a substitute to chemical synthesis. The biosynthesized AuNPs showed antioxidant and antimicrobial activities, demonstrating their utility in biomedical applications. Testing of various other biological applications of these nanoparticles is warranted.

ACKNOWLEDGEMENTS

We acknowledge Sukanya and A. Rajanandhini for their help in conducting this work.

REFERENCES

1. H.M.M. Ibrahim, *Journal of Radiation Research and Applied Sciences* 8 (3) 265–275 (2015).
2. M.M.R. Mollick, et al., *RSC Adv.* 4, 37838–37848 (2014).
3. J.L.G. Torresdey, et al., *Nano Letters* 2 (4) 397–401 (2002).
4. S.A. Masurkar, et al., *Nano-Micro Letters* 3 (3) 189–194 (2011).
5. J. Pulit, and M. Banach, *Bioinorganic Chemistry and Applications* 3569758, 12 (2018).
6. D. Shah, et al., *Materials (Basel)* 8 (11) 7278–7308 (2015).
7. I. Khan, et al., *Arabian Journal of Chemistry* (2017).
8. M. Składanowski, et al., *Journal of Cluster Science* 28 (1) 59–79 (2017).
9. M. Sengani, et al., *Open Nano.* 2, 37–46 (2017).
10. A. Masri, et al., *Antibiotics* 7 (4) 100 (2018).
11. A.D. Mubarak, et al., *Colloids and Surfaces B: Biointerfaces* 103, 166–173 (2013).
12. A.K. Khan, et al., *Tropical Journal of Pharmaceutical Research* 13 (7) 1169–1177 (2014).
13. L.E . Cole, et al., *Nanomedicine* 10, 321–341 (2015).
14. M. Shah, et al., *Materials (Basel)* 8 (11) 7278–7308 (2015).
15. C.J. Murphy, et al., *Acc Chem Res.* 41, 1721–1730 (2008).
16. K.K. Jain, *Neurodegener Dis.* 4 (4) 287–91 (2007).
17. J.F. Hainfeld, et al., *Phys Med Biol.* 49 (18) 309–315 (2004).
18. Y.C. Yeh, et al., *Nanoscale* 4 (6) 1871–1880 (2012).
19. M. Shah, et al., *Frontiers in Bioscience* 19, 1320–1344 (2014).
20. N. Elahi, et al., *Talanta* 184, 537–556 (2018).
21. M. Sett, et al., *Adv. Nat. Sci: Nanosci. Nanotechnol.* 7, 025005 (2016).
22. A. Chowdhury, et al., *International Nano Letters* 7 (2) 91–12 (2017).
23. M.P. Upendra, et al., *Biomedicine & Pharmacotherapy* 97 1521–1537 (2018).
24. P. Singh, et al., *Int J Mol Sci* 19 (7) 1979 (2018).
25. V. Chaudhary, et al., *J Nanobiotechnology* 16, 40 (2018).
26. S. Rautray, et al. *Mol Biol Rep* (2018).
27. X.F. Yang and X.Q. Guo, *Analyst.* 126 (6) 928–932 (2001).
28. S. Anandjiwala,et al., *Indian J Pharm Sci* 70 (1) 31–35 (2008).
29. R.J. Ruch, et al., *Carcinogenesis* 10, 1003 (1989).
30. K.B. Pandey and S.I. Rizvi, *Oxid Med Cell Longev* 2 (5) 270–278 (2009).
31. L. Misra, *International Journal of Traditional and Natural Medicines* 2 (1) 27–75 (2013).
32. A.G. Atanasov, et al., *Biotechnol Adv.* 33 (8) 1582–1614 (2015).
33. A.C. Burdusel, et al., *Nanomaterials* 8, 681 (2018).
34. A. Henglein, *J. Phys. Chem.* 97 (21) 5457–5471 (1993).
35. C. Jayaseelan, et al., *Industrial Crops and Products* 45, 423–429 (2013).
36. J.S. Kumar, et al., *Biochem Biophys Rep.* 11, 46–57 (2017).
37. L.A. Levchenko, et al., *Russ Chem Bull* 60, 426 (2011).
38. T. Elavazhagan and K.D. Arunachalam, *Int J Nanomedicine* 6, 1265–1278 (2011).
39. A.A.A. Aljabali, et al., *Nanomaterials* 8, 174 (2018).
40. D. Lin, et al., *Molecules* 21, 1374 (2016).
41. H. Shabestariana, et al., *Materials Research.* 1–7 (2016).
42. B. Kumar, et al. *Biol Med (Aligarh)* 8, 3 (2016).
43. M.H. Oueslati, et al., *Arabian Journal of Chemistry* (2018).
44. E. Rollet-Labelle, et al., *AFRM* 24, 563–572 (1998).
45. S. Medhe, et al., *Appl Nanosci* 4, 153 (2014).
46. S.R. Guntur, et al., *Anal Chem Insights* 13, 1177390118782877 (2018).
47. A. Chahardoli, et al., *Artificial Cells, Nanomedicine, and Biotechnology* 46 (3) 579–588 (2018).
48. A.A.A. Aljabali, et al., *Nanomaterials* 8, 174 (2018).
49. D. Dang, et al., *Int J Res Med Sci.* 7 (4) 1171–1177 (2019).
50. C. Sreelakshmi, et al., *Journal of Nanoscience and Nanotechnology* 11, 6995–7000 (2011).
51. X.F. Zhang, et al., *Int J Mol Sci.* 17 (9) 1534 (2016). ◆